ACE-FTS Instrument Detailed Design

Marc-Andre Soucy*, Francois Chateauneuf, Christophe Deutsch, Nicolas Etienne
ABB Bomem Inc., Radiometry Division, 585 Charest East, Suite 300, Québec, QC, Canada, G1K 9H4

ABSTRACT

The Atmospheric Chemistry Experiment (ACE) is the mission selected by the Canadian Space Agency for its next science satellite, SCISAT-1. ACE consists of a suite of instruments in which the primary element is an infrared Fourier Transform Spectrometer (FTS) coupled with an auxiliary 2-channel visible (525 nm) and near infrared imager (1020 nm). A secondary instrument, MAESTRO, provides spectrographic data from the near ultra-violet to the near infrared, including the visible spectral range. In combination the instrument payload covers the spectral range from 0.25 to 13.3 micron. A comprehensive set of simultaneous measurements of trace gases, thin clouds, aerosols and temperature will be made by solar occultation from a satellite in low earth orbit. The ACE mission will measure and analyse the chemical and dynamical processes that control the distribution of ozone in the upper troposphere and stratosphere. A high inclination (74 degrees), low earth orbit (650 km) allows coverage of tropical, mid-latitude and polar regions.

This paper describes the detailed design of the ACE-FTS instrument. The principal design drivers and trade-offs are covered as well as system engineering approaches to optimise the performance of the instrument. Its highly folded, compact and robust opto-mechanical design is described. The structural and thermal design challenges, which have considerably impacted the detailed design of the instrument, are presented. Lessons learned during the detailed design phase and manufacturing of the Flight Model are presented. The latest status of the flight model is also presented as well as preliminary test results.

Keywords: ACE, FTS, SCISAT-1, Infrared, Spectrometer, Fourier, Detailed Design

1. INTRODUCTION

The ACE-FTS instrument is composed of a Fourier Transform Spectrometer (FTS) and two imager detectors. The solar occultation measurement technique consists in measuring the solar radiance at sunrises and sunsets. At those moments, the solar radiance is partially attenuated by the chemical components present in the atmosphere. A set of exo-atmospheric spectra and images are also taken as reference measurements. By taking the ratio of these two readings, scientists can identify the specific portions of the Sun's energy that has been absorbed by the Earth's atmosphere thus computing the transmittance of the atmosphere. This information can then be used to determine the chemical constitution of the atmosphere, for altitudes varying between 10-100 km to then improve the understanding of atmospheric ozone and the chemicals responsible for its destruction. The main instrument is a high-resolution (0.02 cm^{-1}) infrared Fourier Transform Spectrometer (FTS) operating in the 750 to 4100 cm^{-1} spectral range.

The Principal Investigator is Dr. Peter Bernath from the Department of Chemistry at the University of Waterloo. He heads a Science Team that includes Canadian scientists as well as scientists from the United States, Belgium, Japan, France and Sweden. ABB-Bomem inc. is the industrial prime contractor for the development of the ACE-FTS main instrument. The spacecraft bus is being built by Bristol Aerospace. SCISAT-1 is scheduled for launch by NASA in December 2002.

The main design drivers of the ACE-FTS instrument are sensitivity (SNR), spectral resolution and large spectral coverage. The principal constraints were the available volume, mass and power consumption from the spacecraft bus. The instrument has also to cope with a challenging vibration and thermal environment. One key requirement of the program is to design and manufacture a low cost, quickly-developed instrument while keeping the risks as low as possible. As described in the following pages, the double-pass interferometer design was the selected approach to meet those objectives. The instrument also takes advantage of the solar occultation technique, which allows very good signal levels while reducing the criticality for long-term instrument stability requirements and the need for on-board calibration sources. The Figure 1 shows the first spectrum acquired by the ACE-FTS Instrument (Flight Model) during the start-up phase and a photo taken during the integration phase.

*Author to whom correspondence may be addressed: Email : marc-andre.a.soucy@ca.abb.com; Telephone : 418 877 2944
SCISAT-1/ACE Web Site: www.science.sp-agency.ca/J3-SCISAT-1.htm

Earth Observing Systems VII, William L. Barnes, Editor,
Proceedings of SPIE Vol. 4814 (2002) © 2002 SPIE · 0277-786X/02/$15.00

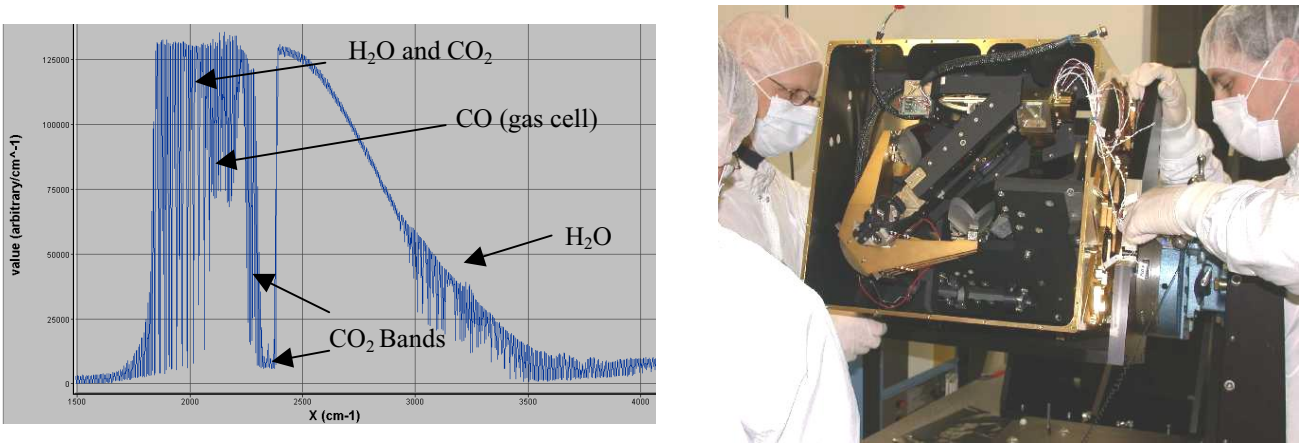

Figure 1 : First spectrum measured (non-corrected, cold source, InSb band) with the ACE-FTS instrument flight model (left) and photo during instrument integration phase (right)

The principal goal of the Atmospheric Chemistry Experiment (ACE) mission is to measure and understand the chemical and dynamical processes that control the distribution of ozone in the upper troposphere and stratosphere. Human activity is causing changes in atmospheric ozone concentrations and is increasing the amount of ultraviolet radiation received by Canadians. The ACE mission is focussing on one important and serious aspect of the atmospheric ozone problem – the decline of stratospheric ozone at northern mid-latitudes and in the Arctic.

Average ozone declines have been measured over much of Canada using ground-based Brewer spectrophotometers[1]. Since 1980 all five long-term Canadian stations (including Toronto 44° N, 79° W) have found a statistically significant decrease of about 6% in the ozone column. Ozone sonde measurements show that most of the decline has occurred in the lower stratosphere and the current atmospheric models cannot account for these observations. The total ozone column obtained from satellite-based TOMS instruments shows that in March 1997, the ozone column was 21% less than normal and in a small region near the pole the decrease was 40%[2]. The only reasonable explanation for this data is chemical loss of ozone probably due to heterogeneous chemistry. The goal of ACE is to help explaining these losses.

2. ACE-FTS INSTRUMENT OVERVIEW

The ACE primary instrument is an infrared Fourier Transform Spectrometer (FTS) coupled with an auxiliary 2-channel visible and near infrared imager. The FTS, operating from 2.4 to 13.3 microns, measures at high resolution (0.02 cm^{-1}) the infrared absorption signals that contain information on different atmospheric layers to provide vertical profiles of atmospheric constituents. Its highly folded design results in a very high performance instrument with a compact size. The imager monitors aerosols based on the extinction of solar radiation using two filtered detectors at 1.02 and 0.525 microns. The spectrometer is an adapted version of the classical Michelson interferometer using an optimised optical layout. A signal-to-noise ratio (SNR) better than 100 is achieved, with a field-of-view (FOV) of 1.25 mrad and an aperture diameter of 100 mm. Finally, the instrument includes a suntracker, which provides fine pointing toward the radiometric centre of the Sun with a stability better than 15 μrad, to both the infrared spectrometer and the imager during solar occultation of the Earth's atmosphere.

The instrument optical layout is illustrated in Figure 2. The first optical item is the suntracker module, which tracks the radiometric centre of the sun. The infrared and visible signals are then sent to the telescope primary mirror, which provides a magnification factor of 5X. A small 1.55 μm filter is mounted on the telescope mirror. Its function is to transmit that wavelength to the quad cell used as the feedback source for the suntracker module (located behind the telescope primary mirror) and to reflect the remaining spectrum to the Vis/NIR imager. In addition to that, each imager has its own filter to extract each wavelength with a bandwidth of 1 %. This design simplifies the quad cell and Vis/NIR imager optical interfaces. The primary mirror then transmits the signals to the aperture and field stops. After the stops, the secondary mirror collimates the beam to the interferometer and a filter is used to minimise the thermal load on the interferometer. When the 6.25 mrad divergent infrared signal enters the interferometer, it is split in two parts going in each interferometer arm. The signals are reflected back to the beamsplitter using cube-corners with flat mirrors in front of them. This additional reflection is provided by the end mirror, which has also a hole on its centre to transmit the modulated signals to the detector/cooler sub-

system. This novel configuration allows optical components to be compensated for tilt and shear. The recombination of the infrared signals at the beamsplitter level provides interference since the OPD is changed (±25 cm) by the actuated rotary arm of the interferometer sub-system.

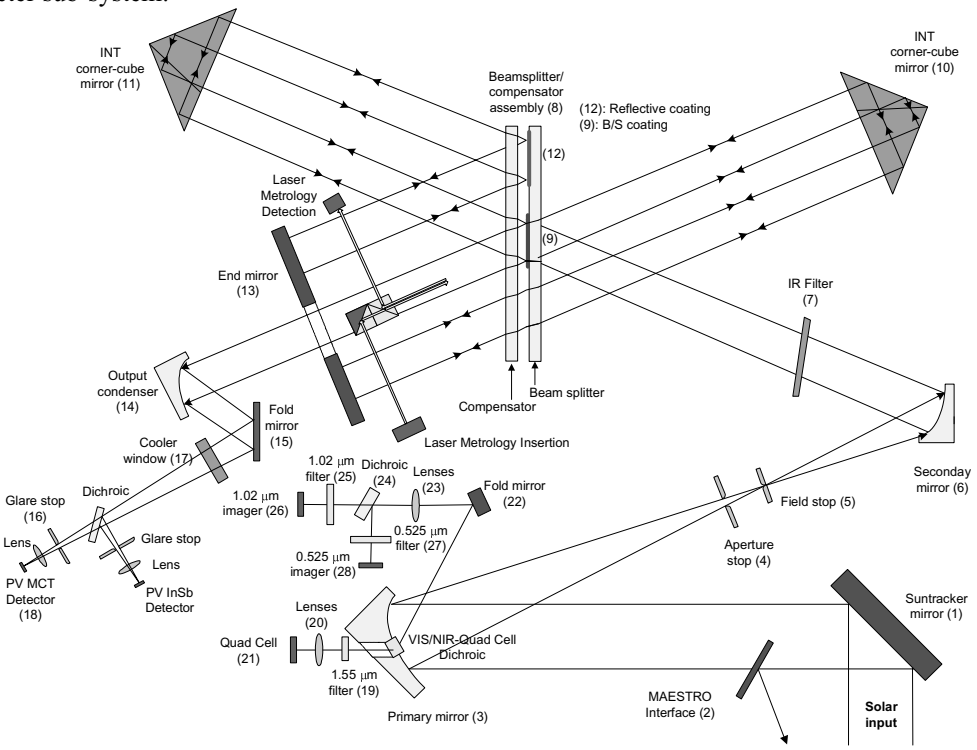

Figure 2: ACE-FTS instrument optical layout

The output of the interferometer is then condensed to the InSb/MCT detector using another off-axis parabola. The Instrument Electronics sub-system controls the instrument, the rotary arm motion, interferogram/imager sampling, housekeeping monitoring and data formatting. Both science data and additional data (housekeeping, spacecraft) are then down-linked to the ground after CCSDS packetization. The raw data (level 0) is then received at the ground station level. Level 1A and 1B data processing is then performed to obtain spectrally calibrated, geo-located, transmittances of the atmosphere.

3. INSTRUMENT DETAILED DESIGN

The main design drivers of the ACE-FTS instrument are sensitivity (SNR), spectral resolution and large spectral coverage. The principal constraints were the available volume, mass and power consumption of the spacecraft bus. The instrument has also to cope with a challenging vibration and thermal environment. One key requirement of the program is to design and manufacture a low cost, quickly-developed instrument while keeping the risks as low as possible. The double-pass interferometer design, as illustrated in Figure 2, was the selected approach to meet those challenging objectives.

The next sub-sections describe the key considerations of the optical, mechanical and electrical detailed design of the instrument.

3.1. Optical design overview

One of the main requirements of the optical design was simplicity and compact packaging. In order to package the optics in a relatively small volume, a three-dimensional approach was selected. A direct consequence of three-dimensional packaging is the difficulties in accessing components for alignment. In order to cope with this difficulty, it was therefore important that optical interfaces between instrument sub-systems be provided by collimated beams allowing easy alignment, monitoring, test and larger tolerancing. The high sensitivity requirement, particularly when considering the high spectral resolution

(0.02 cm^{-1}) and large spectral coverage (750-4100 cm^{-1}) of the instrument, was also a difficulty. The high solar flux entering the instrument, and consequently thermal load variations, was an important design factor to ensure good optical stability.

There are two ways to conceive a radiometer system depending on what is imaged at the detector. An imaging system (camera for example) is required to have the image of the scene onto its detector. For a radiometer or photometer another possibility is to place the detector at the exit pupil, the final image of the aperture stop. It could be the aperture stop as well. While having neither is also possible from a radiometry point-of-view, we would not fulfil the condition that the detector size is minimised from the throughput conservation principles. This last factor insures minimal detector noise contribution and is crucial for sensitivity performance. The pupil is typically uniformly illuminated if the source is lambertian even if it has structure or non-uniformity. One exception is the obscuration of Cassegrain telescope like on ACE. This is however always present and can be calibrated out like the other transmission factors in the instrument. The other factor to consider is the detector non-uniformity. While some detector types utilise rather pure materials (InSb) which gives them rather uniform response over their area, others (MCT) exhibit a certain degree of non-uniformity.

The field imaging approach projects the scene image onto the detector. It is therefore straightforward to see that there is a multiplication of the scene and detector non-uniformity and that moving slightly the scene on the detector could lead to a change in the measurement while the scene remains in fact unchanged. The image uniformity at the detector is poor seeing that it is very influenced by the field of view, therefore, sensitive to "pointing" errors. The main drawback of field imaging is its very high sensitivity to translation in the field plane since little variations on this will cause image quality degradation. Considering the large solar heat loads on the field stops, this is quite a serious issue. On the other hand, the pupil imaging approach is sensitive to aperture stop and focusing variations.

Considering all the points above and other ones, the pupil imaging optical design approach was selected to obtain a better uniformity and a smaller detector (therefore higher sensitivity). To maximise stability, all components with optical power, exposed to temperature variations, are reflective. An off-axis telescope design has been retained for simplicity. The 6.25 mrad divergence in the interferometer is optimised up to the limit of the ILS FWHM requirement (< 0.028 cm^{-1}), resulting in a telescope magnification factor of 5. In order to optimise the sensitivity and accuracy of the instrument, the spectral range is divided in two bands using InSb and MCT detectors. The high level of energy on the MCT detector led to a photo-voltaic (PV) detector instead of photo-conductive (PC), reducing considerably the non-linearity effects. All refractive optics in the instrument are wedged to reduce channel spectrum. Errors in evaluation of atmospheric transmittance due to channel spectrum variations resulting from thermal drifts in the beamsplitter of the interferometer were estimated to be less than 0.05%. The optical design of the ACE-FTS instrument is under the diffraction limit. The Figure 3 illustrates the main components of optical design of the instrument (only one arm of the interferometer shown, VNI imager not shown).

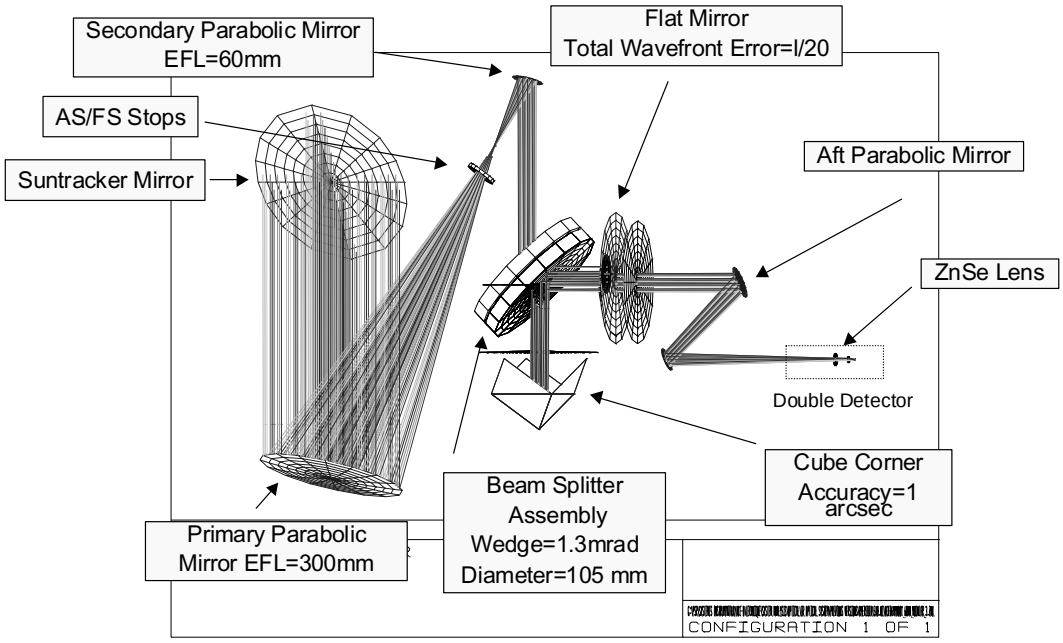

Figure 3 : Instrument optical design (only one interferometer arm shown, VNI imager not shown)

The suntracker, supplied by Ball Aerospace, provides the FOV tracking to the centroid of the sun to a stability better than 15 µrad. The suntracker has a field-of-regard (FOR) of ±5 degrees, and is actively controlled using a quad cell detector as feedback. The FTS aperture and field stops are positioned after the main parabola and define completely the FTS 1.25 mrad field-of-view (FOV) and optical axis. Their relative closeness provides the required FOV and instrument line shape stability that would have been hardly achievable if they were put apart on each side of the FTS. A very important consideration was the heat rejection of the aperture and field stops, needed to ensure good optical stability. A parabolic-shaped field stop was designed to reject as much as possible undesired radiation. The stops are also mirror-quality manufactured to reflect efficiently the light out of the FOV of the instrument. The Figure 4 shows the aperture/field stop design and comparison of absorbed power when comparing full power (or full absorption using black coatings) and the selected parabolic mirror coating design.

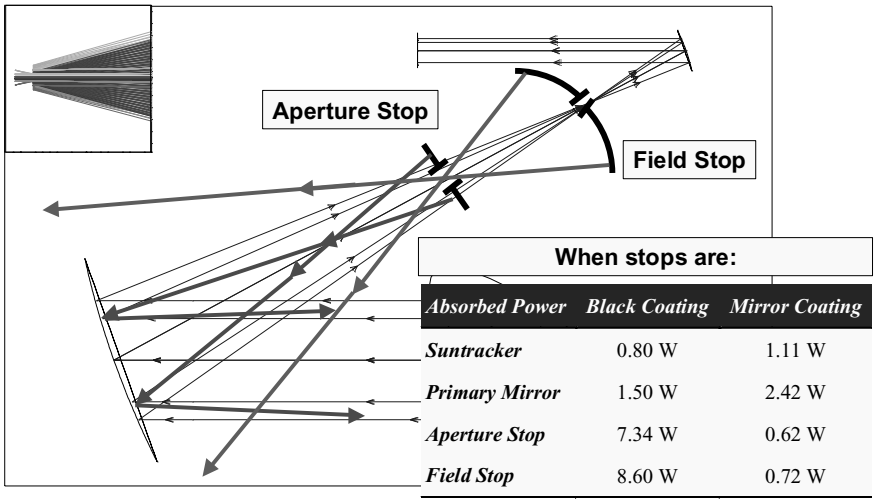

When stops are:

Absorbed Power	*Black Coating*	*Mirror Coating*
Suntracker	0.80 W	1.11 W
Primary Mirror	1.50 W	2.42 W
Aperture Stop	7.34 W	0.62 W
Field Stop	8.60 W	0.72 W

Figure 4 : Design of aperture and field stops using parabolic mirror coatings to minimise heat load

The optical design of the interferometer sub-system is highly folded, fully compensated, and insensitive to the tilt and shear of any of its components. Though retro-reflectors are used, the ACE-FTS is in fact a flat-mirror interferometer and no shear of the interfering beams is induced by a misalignment of the retro-reflectors. The compensation and tilt insensitivity is even preserved in the presence of a wedge mismatch between the beamsplitter and the compensator substrates or of a wedged air gap. This robustness is made possible by the fact that both optical paths hit a common end mirror and that a tilt of this optical component affects them in an exact similar way. However, this design does not only offer advantages and it possesses in fact minor side effects that have been considered, such as beamsplitter thickness mismatch, imposing a temperature stability of 500 mK to the beamsplitter-compensator assembly during the solar occultation period. The interferometer and the input optics sub-systems are shown at Figure 5.

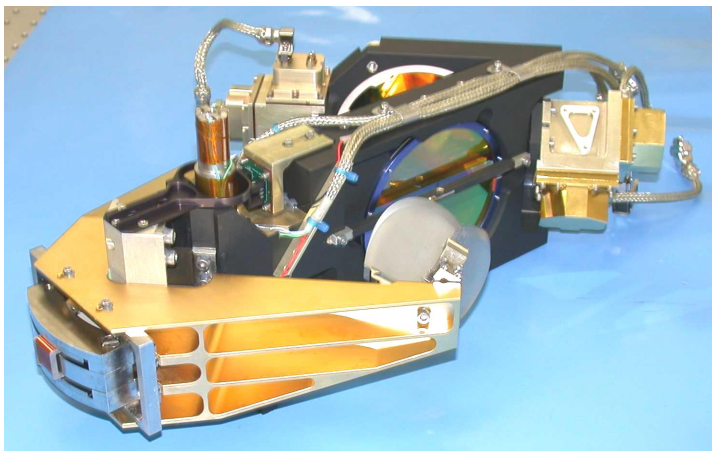

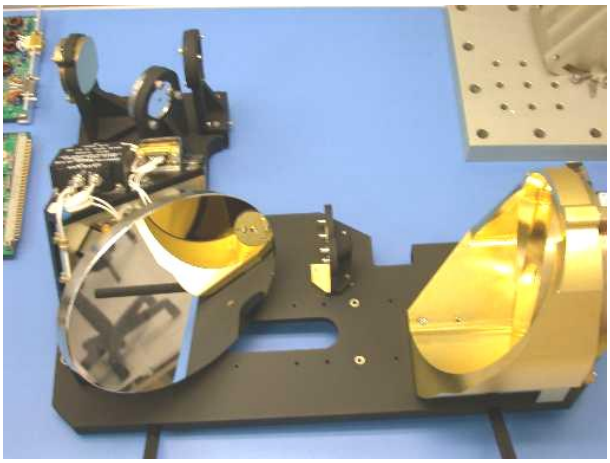

Figure 5: Interferometer sub-system (left) and input optics sub-system (right)

A redundant 1550 nm solid-state distributed feedback laser diode is used as the metrology source. The current and temperature of the metrology laser are controlled to obtain wavelength stability better than 0.024 ppm for the 2-second sweep period and 0.3 ppm over the 3-minute occultation duration. The metrology injection and detection optical interface is provided by the use of a prism mounted on the end-mirror of the interferometer.

The infrared detector of the ACE-FTS instrument is a side-by-side configuration of two photo-voltaic detectors, one InSb and one HgCdTe. The sensitivity of the detectors is very critical in order to meet the NESR requirement (or SNR on transmittance spectra). The instrument has been designed to maximise the solar flux on the detectors. As a result, the detectors suffer of non-linearity, which impacts the transmittance accuracy of the instrument. This is however mitigated by the use of photo-voltaic (PV) detectors. The detectors are cooled using a passive cryo-cooler, provided by Ball Aerospace. The aft-optics inside the detector/cooler sub-system provides pupil re-imaging. The opto-mechanical design of the aft-optics has been optimised to ensure that the alignment is kept over the entire thermal range of that sub-system. The off-axis parabola in the aft-optics provides diffraction limited performance. The cooling performance of the passive radiator was measured between 78 and 98 Kelvins depending on orbital configurations simulated in the thermal-vacuum chamber. The earth shield of the detector/cooler sub-system as an optimised geometry to reduce the earth backloading on the cold radiator, particularly for high orbital Beta angles. The Figure 6 shows the detector/cooler sub-system.

Figure 6 : Detector/cooler sub-system

To ensure good modulation efficiency, the double-pass design requires very good optical quality for the cube-corners (orthogonality) and the end mirror (flatness). The orthogonality performance of the cube-corners is 1 arc-sec at room temperature. In addition of impacting modulation efficiency, variations of the cube-corner distortion over the occultation period induce transmittance errors. The end-mirror flatness is also very critical to ensure that no wavefront errors are introduced.

A problem was discovered during preliminary testing of the Flight Model, impacting seriously the modulation efficiency performance. The issue was related to the mounting of the end-mirror of the interferometer, which was causing a significant deterioration of its flatness. This problem was corrected by adding RTV axial pads and the measured modulation efficiency is now between 80 and 99% for the whole spectral range (requirement > 70%). The Figure 7 illustrates the flatness of the end-mirror as obtained by a Zygo measurement. The flatness before cell mounting was measured 64 nm peak-to-valley (mirror alone) and was measured at 67 nm peak-to-valley after mounting inside its Invar cell. The 3 nm ($\lambda/200$) flatness error introduced by the mounting is therefore extremely low.

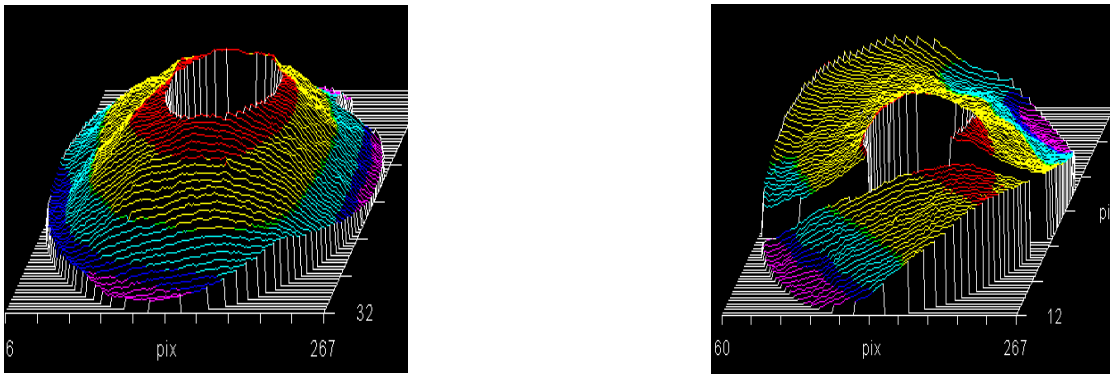

Figure 7: End mirror flatness of 64 nm P-V before mounting (left), and of 67 nm P-V after mounting inside its cell (right)

3.2. Mechanical design overview

The structural design of the instrument has to comply with several factors. The mass of the instrument has to be as low as possible. At the same time, the structure is required to provide a stable temperature environment and a stable mounting to the spacecraft bus. Finally, the structure has to resist to the vibration environment associated with the launch of the spacecraft. The combined parameters of rigidity, cost and mass indicated that the structure was to be machined from a single large block of 6061-T6 Aluminium. Extensive use of ribbing patterns on both the inside and the outside of the structure allowed to save even more mass while providing the required stiffness. Finally, the instrument structure was thermally de-coupled from the spacecraft base-plate in order to provide better thermal control.

3.2.1 Structural design overview

This challenging multidisciplinary design has required many months of detailed (up to 140,000 degrees of freedom) structural and thermal finite element analyses (FEA). Most FEA were correlated by testing, and many opto-mechanical trade-offs were performed in order to accommodate the optical, electrical, servo and system requirements. The ACE-FTS instrument is designed to resist to the vibration loading derived from the coupling of the SciSat-1 spacecraft to the Pegasus XL launch vehicle and then the thermal loading while in orbit. The Figure 8 illustrates the structural Finite Element Model (FEM) of the instrument.

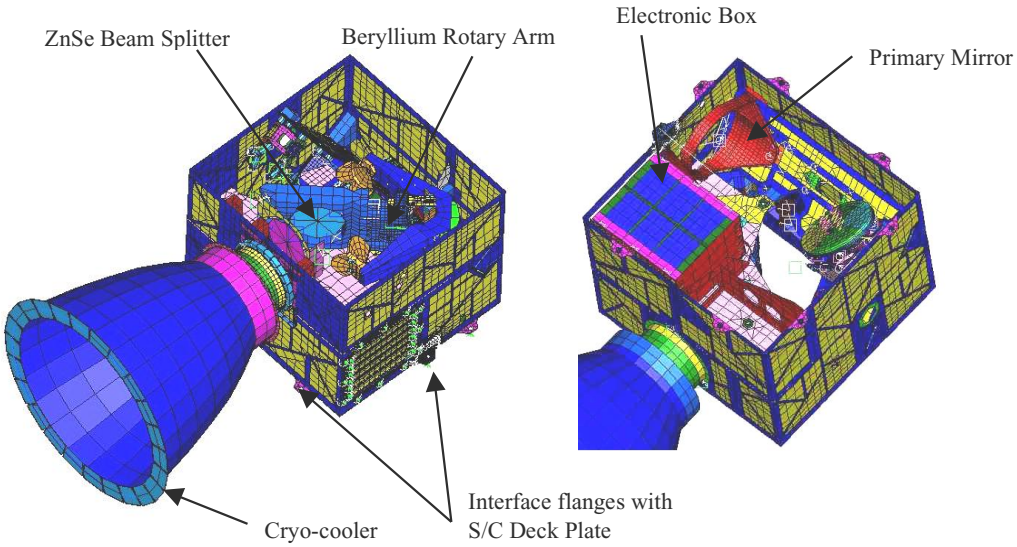

Figure 8 : Instrument structural Finite Element Model

In order to validate the FEA, many sub-systems tests were performed and then accurate correlation was established particularly regarding damping ratios. FEM viscous damping has been adjusted to 1.25%. The Figure 9 shows a correlation of FEA model and vibration testing in one axis of the instrument structure sub-system.

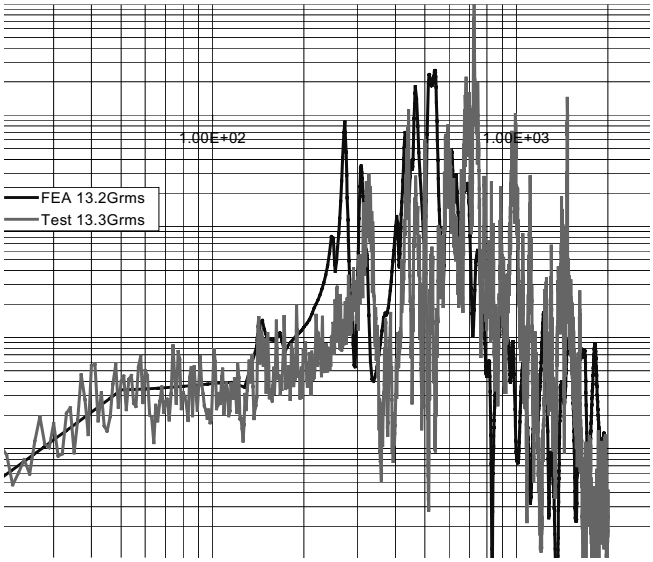

Figure 9 : Typical FEA/test correlation result (in this case, instrument structure sub-system)

FEA dynamic response measurements provide more realistic stresses evaluation of components. Every power spectrum density curves applied during vibration tests on shaker was calculated at corresponding interfaces from the detailed FEM. Tests are very complimentary to FEA, first for validating the simulation results themselves and particularly for verifying components that cannot be modelled accurately (adhesive shear resistance on coated cell for example).

Two very critical components with respect to vibration survivability are the cube-corners (retro-reflectors) used in the interferometer sub-subsystem. The Flight Model (FM) cube corners are different than the ones used in the Engineering Model (EM). The FM cube-corners have been specifically designed for high vibration loads. The assembly of the Zerodur optical mirrors of the retro-reflectors is achieved using a special tripod mounting structure including flexures. The material used for the mounting structure of the cube-corners was selected to be very thermally stable. Test and spare components were procured and tested for random vibration (bandwidth 20-2000 Hz, 60 seconds, lateral at 46g rms and axial at 29.7g rms). The levels used for vibration testing of the cube-corners were derived from the instrument-level FEA. The cube-corners survived to the proto-qualification environment and no visible damage or deformation was observed.

Another vibration-critical component of the instrument is the flexure-based mechanism of the interferometer sub-system. The very large Optical Path Difference (OPD) needed to achieve the 0.02 cm^{-1} spectral resolution has raised some challenging problems on the opto-mechanical aspects of the design. In fact, despite the highly folded optical design, which translates into a factor of eight (8) between the mechanical and optical sweeping speeds and travel range, the stroke of the rotary arm has to cover a ± 15° range. A new flexure design had therefore to be developed to face the high vibration loads as well as fatigue stresses due to bending over the 2-year mission duration.

Trade studies have been conducted to design fatigue resistant flexures that will survive the vibrations of the spacecraft launch. Thinner flexures present a low torsional stiffness therefore requiring less power consumption. They are however weak and do not survive the launch stress where the buckling and fatigue cycles loading tear them apart. Along the fatigue and vibration test path, the flexure design went from spring steel (C1095) blades through titanium (Ti 6Al-4V) and finally stainless steel (SS 17-7 CH900). Even with this material, the dynamic loading on the blades was still too high and the mass of the whole rotary arm had to be reduced in order to meet the vibration requirements imposed by the launch. This was achieved by machining a beryllium rotary arm instead of aluminium. Special attention was also needed for the staking method of the flexures. More than a dozen of iterations and vibration tests were needed before obtaining the final flexure design configuration.

A test jig was built to test the flexures of the rotary arm, as illustrated in Figure 10. Vibration tests were performed on the rotary arm flexures to a bandwidth of 20-2000 Hz, for duration of 60 seconds, and at a 13g rms load vertical, which is the worst case for buckling. The same vibrated assembly was then cycled during several weeks on a test bench to simulate the fatigue of the orbital life. The flexures survived to the vibration tests and cycling and kept their nominal characteristics. It is important to mention that dynamic buckling is difficult to model with FEA.

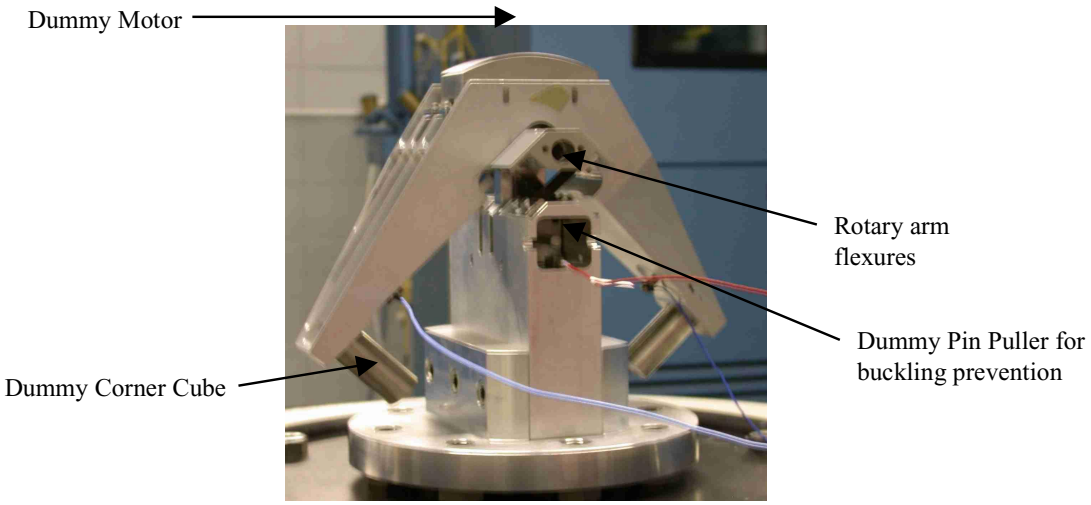

Figure 10 : Vibration test setup of interferometer rotary arm flexures

Vibration tests were also successfully performed on the laser diode source assembly, to a load of 20g rms. The alignment was also verified as well as survivability of the thermo-electric coolers used for the thermal control of the laser diodes. The complete laser source assembly involves nearly 200 opto-mechanical components. Vibration tests were also performed on the FTS/spacecraft bus interface G10 sleeves. Complementary vibration tests were performed at the Canadian Space Agency for the validation of G10 elastic and damping properties. Since these thermal and structural components link the instrument and the spacecraft bus, the interface dynamic transmissibility must be known more accurately. A sine test (0.25G) was performed in three dimensions in order to determine equivalent analytical tri-axial spring element for FEA model. After correlating the test with an equivalent FEM, we now use the new spring values in the detailed FEM.

3.2.2 Instrument thermal design overview

One of the most challenging thermal engineering activities of the ACE project was to reduce the operating temperature excursion of the instrument with very limited active heating power. The instrument is exposed to various orbital environments and varying end-of-life thermal isolation material characteristics. The instrument is isolated with G10 posts and titanium fasteners from the spacecraft bus, which results in a wider temperature range. A radiator sized with precision allows the solar absorbed energy and electrical power to be dissipated, while keeping reasonable thermal hot/cold case excursions for the various orbital configurations. Moreover, optical components with different coefficient of thermal expansion than aluminium are bounded with adhesive of calibrated thickness to achieve athermal joints. Temperature sensitive components like cube-corners are isolated from the rest of the instrument by mean of flexure blades and low emissivity coatings. One important aspect of the thermal design is the passive radiator of the infrared detectors, as described in Section 3.1.

The Figure 11 illustrates the simplified thermal model. The detailed thermal model, containing 5,856 elements, was very useful to optimise thermal stability by selecting appropriate surface finishes, materials, adhesives, etc. The Figure 12 presents the key parameters of the thermal analysis while the Figure 13 shows the cold case, hot case and survival case results. The thermal performance of the Flight Model will be verified during the acceptance testing phase of the instrument in thermal-vacuum chamber (TVAC).

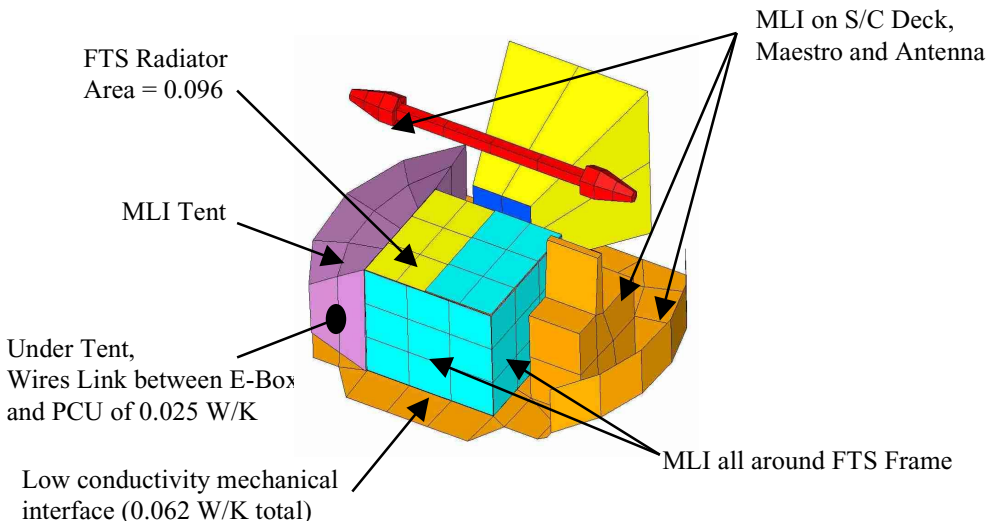

Figure 11 : Instrument thermal model (simplified model)

	Right Ascension of Ascending Node	FTS Radiator Silver-Teflon Tape Emissivity	FTS Radiator Silver-Teflon Tape Solar Aborptivity	MLI Effective Emissivity	Kapton Outer Layer Emissivity	Kapton Outer Layer Solar Absorptivity	Electrical Mean power (with heater power)	Input Optics Absorbed Solar Mean power	Solar Intensity	Albedo	Earth IR	Baseplate Temperature	PCU Temperature
	β (Degree)	**$\varepsilon_{Radiator}$**	**$\alpha_{Radiator}$**	**ε^*_{MLI}**	**ε_{Kapton}**	**α_{Kapton}**	**P_E (W)**	**P_S (W)**	**S (W/m^2)**	**A (%)**	**E_{IR} (W/m^2)**	**T_{Base} (°C)**	**T_{PCU} (°C)**
Operation Cold Case	0	0.79	0.05	0.05	0.78	0.45	19.6	6.2	1290	31.6	213.9	-10	-15
Operation Hot Case	53	0.79	0.20	0.01	0.78	0.55	17.0	8.1	1420	39.6	239.1	40	40
Survival Cold Case	90	0.79	0.05	0.05	0.78	0.45	9.5	0	1290	31.6	213.9	-50	-50

Figure 12 : Thermal model key parameters

	β Angle (Degree)	Mean Frame Temperature (°C)	Hottest Point Temperature in Optics (°C)	Coldest Point Temperature in Optics (°C)	Temperature at Radiator (°C)
Operation Cold Case	0	7.4 to 8.4	7.5 to 13.0 at Aperture Stop	4.4 to 5.0 at Retro-Reflector	-2.0 to 3.0
Operation Hot Case	53	24.5 to 25.2	24.7 to 31.0 at Aperture Stop	20.5 to 21.6 at Retro-Reflector	16.0 to 19.4
Survival Cold Case	90	-39.4	-39.7	-43.0	-43.0

Coldest temperature

Hottest temperature

Figure 13 : Thermal model cold case, hot case and survival case results

3.3. Electrical design overview

The Instrument Electronics sub-system is composed of six (6) Circuit Card Assemblies (CCAs) integrated in a common enclosure and interfacing via a backplane. A redundant power supply unit is also integrated in the same enclosure. The CCA-1 provides serial interfaces with the spacecraft bus and data formatting, by the Instrument Data Formatter (IDF) FPGA. Commands are also interpreted by the Instrument Control Unit (ICU) FPGA. The sub-systems are then controlled according to the commands received from the platform. Reading of the Vis/NIR imager is performed as well as an on-board cropping algorithm to reduce the data rate of the 30 mrad images. Typical images of the Sun only cover a sub-section of the 128×128

image. In fact, the imager FOV is 30 mrad while a non-refracted Sun sustains a 9.6 mrad angle. The cropping algorithm has to cope with atmospheric effects such as vertical compression of the Sun image due to refraction in the atmosphere. The CCA-1 also provides reading of housekeeping signals such as temperatures, voltage levels, laser power & current, suntracker mirror positions, etc.

The CCA-2 provides position-control of the rotary arm in a closed-loop configuration. The position profile is generated by a FPGA. A Proportional-Integrator-Derivative-Filter (PIDF) servo compensation is implemented and is coupled by a feed-forward controller. Actuator power drive is also provided by CCA-2. The figure below illustrates the block diagram of the servo system.

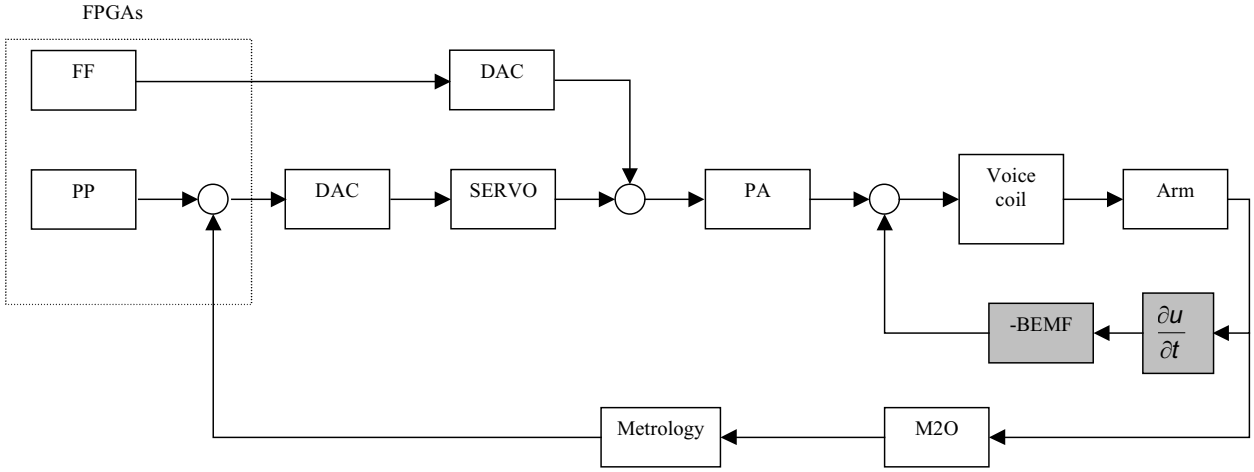

Figure 14 : Servo control of the interferometer rotary arm

In the above diagram, the FF is the feed-forward profile, PP is the position profile, SERVO is an analogue PIDF, PA is the power amplifier, BEMF is the back electromotive force due to the displacement of the coil and M2O is the mechanical to optical conversion. The process model has been identified analytically, and verified using a dynamic signal analyser. The Figure 15 illustrates the frequency response of the rotary arm of the interferometer (measured versus model).

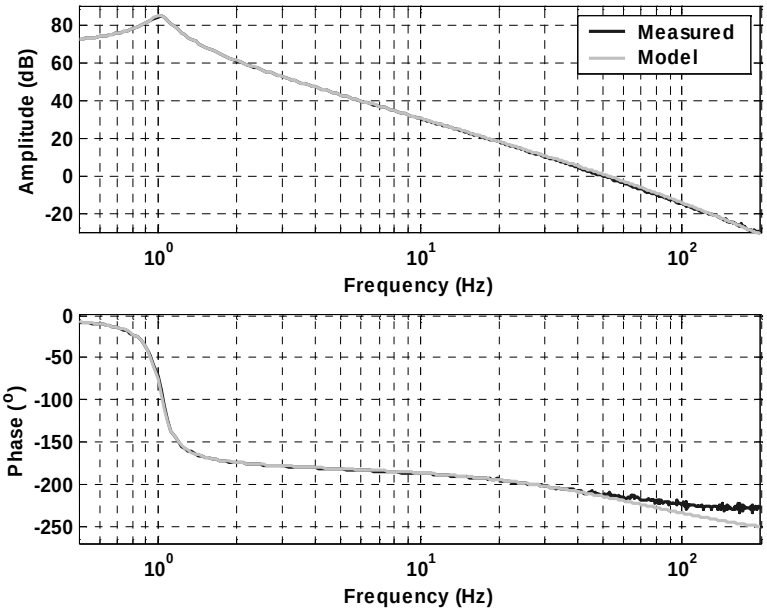

Figure 15 : Bode plots (model versus measured) of the rotary arm

The speed stability of the interferometer was measured and is better than 0.05% RMS (20 times better than requirements) confirming very good servo control of the rotary arm. As shown by Zachor[3], the speed instability could be an important source of noise for an FTS. The phase margin of the servo system is 36 degrees and the gain margin is 24 dB.

The CCA-3 provides acquisition of the infrared data (InSb/MCT detectors). Dual ADC approach is used to cope with the high dynamic range and reduce the noise contribution of the digitisation. The ACE Phase A study showed the need of a space qualified ADC of at least 17 bits to sample the infrared interferogram in order to bring the digitisation noise below the other noise contributors. To get around the availability issue of space-qualified 17-bit ADCs, a positional gain switching technique with dual ADC channels is used where the gain of the ADC is raised when the optical path difference lies beyond a certain value while a smaller gain is used in the Zero-Path Difference (ZPD) region of the interferogram. The CCA-4 provides the control of the suntracker and the CCA-5/6 are the redundant power supply boards, supplied by EMS Technologies, providing the needed voltage levels using the +28V from the spacecraft bus.

4. CONCLUSION

The ACE-FTS on-board of the SCISAT-1 spacecraft will provide spectrally calibrated, geo-located, transmittances of the atmosphere. The high-level requirements of the program have resulted in several challenges that were reflected in the detailed design of the instrument. The Flight Model instrument is presently in acceptance and environmental test phase. The first spectra have been acquired and preliminary results are very encouraging. The SNR, spectral resolution, modulation efficiency and ILS preliminary measurements are over the requirements. Preliminary results indicate that most requirements will be met to the exception of few minor non-compliance. The instrument will be integrated to the spacecraft bus in July 2002. SCISAT-1 is scheduled for launch by NASA in December 20th, 2002.

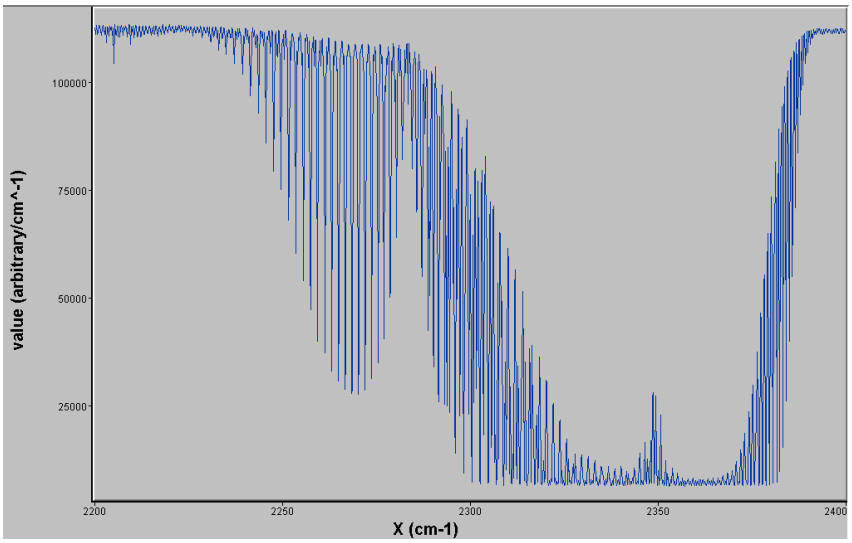

Figure 16 : CO_2 bands measured with Flight Model (cold blackbody source, short-wave band)

ACKNOWLEDGMENTS

The authors would like to thank all the persons involved in the design, manufacturing, testing and management of the ACE-FTS instrument. Over 150 people have contributed to the realisation of this instrument; we are indebted to all of them.

REFERENCES

1. D. I. Wardle, J. B. Kerr, C. T. McElroy, and D. R. Francis, "*Ozone Science: A Canadian Perspective on the Changing Ozone Layer"*, Environment Canada, 1997.
2. P. A. Newman, J. F. Gleason, R. D. McPeters, and R. S. Stolarski, Geophys. Rev. Lett., **24**, 2689, 1997.
3. A. Zachor, "*Drive nonlinearities: their effects in Fourier spectroscopy*", Appl. Opt. **16**, pp. 1412-1424, 1977.
4. F. Châteauneuf, S. Fortin, C. Frigon and M.-A. Soucy , ABB-Bomem inc., "*ACE-FTS Test Results and Performances*", Proceedings of the SPIE. Vol. 4814, 2002.